Catalysis Science & Technology

PAPER

View Article Online
View Journal | View Issue

Cite this: *Catal. Sci. Technol.*, 2016, **6**, 1064

Structural effects of two-dimensional perovskite $Ca_2Nb_2TaO_{10}^-$ nanosheets for photocatalytic hydrogen evolution†

Kazuhiko Maeda*[a] and Miharu Eguchi[b]

Received 3rd August 2015,
Accepted 21st September 2015

DOI: 10.1039/c5cy01246e

www.rsc.org/catalysis

Restacked nanosheets of Dion–Jacobson perovskite $Ca_2Nb_2TaO_{10}^-$ were studied with respect to the structural features as photocatalysts for H_2 evolution from an aqueous methanol solution. The materials were prepared by the reaction of layered $HCa_2Nb_2TaO_{10}$ with tetra-*n*-butylammonium hydroxide (TBA^+OH^-) at room temperature, followed by restacking with a proper restacking agent. According to structural characterization by means of X-ray diffraction, transmission electron microscopy, Raman spectroscopy, and UV-visible diffuse reflectance spectroscopy, the structural features and the degree of interlayer hydration of the restacked material depended on the restacking agent employed. The highest photocatalytic activity was obtained for the restacked nanosheets using HCl as the restacking agent. Results of structural characterizations and photocatalytic reactions suggested that the high activity resulted from not interlayer hydration but protonation, which is favorable for the oxidation reaction.

1. Introduction

Two-dimensional nanocrystals, so-called nanosheets, have attracted attention for diverse applications.[1] Semiconductor photocatalysis is a typical functionality of metal oxide nanosheets.[2–8] Photocatalytic reactions on a semiconductor are accomplished when electrons and holes, generated in the conduction and valence bands, respectively, are consumed by surface redox reactions.[9] Therefore, physicochemical properties such as crystallinity and morphology are important factors that can affect photocatalytic activity.

Compared to the conventional bulk-type metal oxide semiconductors such as TiO_2, the anisotropic feature of nanosheets having a thickness of 1–2 nm and lateral dimensions of several hundreds of nanometer to micrometers is of interest, due to reduced dimensions that contribute to fast charge separation and migration from the bulk to the surface.[10] Charge separation, which is due to electron transitions from the valence band and the conduction band, occurs in the two-dimensional nanosheet. Therefore, in-plane crystallinity (the lateral size) of the nanosheet has a significant impact on photocatalytic activity, as has been revealed by our previous study.[5a] Dion–Jacobson type metal-oxide nanosheets can be readily re-assembled upon addition of a suitable restacking agent (*e.g.*, acid, base, or salt) into a colloidal suspension of nanosheets. The resulting material consists of aggregated two-dimensional nanosheets, where each nanosheet having negative charge is interleaved by cationic species. The cationic species used for the restacking process may be incorporated into the interlayer space of the nanosheets. For layered compounds, the interlayer nanospace may become an efficient reaction site.[5e,6a,11–13] Ebina *et al.* prepared $Ca_2Nb_3O_{10}^-$ nanosheet aggregates restacked using Li^+, Na^+, or K^+ in the presence of a small amount of ruthenium red to achieve overall water splitting.[2b] According to that report, it was claimed that Na^+-restacked material showed the highest performance for the reaction due to more hydrated interlayers that functioned as reaction sites. Our group recently reported that controlling the band-edge potential of perovskite nanosheets allows one to maximize the photocatalytic activity for H_2 evolution, recording a very high apparent quantum yield (AQY) of ~80% at 300 nm using $HCa_2Nb_2TaO_{10}$.[5d] Ida *et al.* also reported high photocatalytic activities of $HCa_2Nb_3O_{10}$ nanosheets doped with Rh^{3+} or Tb^{3+} for H_2 evolution, with 65% (at 300 nm) and 73% (at 270 nm) AQY, respectively.[7a,d]

Thus, very high AQYs for H_2 evolution from an aqueous methanol solution have been observed in some metal oxide nanosheets, with research focused on effects of in-plane crystallinity (lateral size),[5a] composition in the 2-D sheet (band-edge positions),[5d] and doping of foreign elements.[7a,d] The present work deals with structural effects of the $Ca_2Nb_2TaO_{10}^-$-based nanosheet for H_2 evolution. In particular, effects of interlayer cationic species on structure and

[a] *Department of Chemistry, Graduate School of Science and Engineering, Tokyo Institute of Technology, 2-12-1-NE-2 Ookayama, Meguro-ku, Tokyo 152-8550, Japan. E-mail: maedak@chem.titech.ac.jp*
[b] *Electronic Functional Materials Group, Polymer Materials Unit, National Institute for Materials Science, 1-1 Namiki, Tsukuba, Ibaraki 305-0044, Japan*
† Electronic supplementary information (ESI) available: Additional characterization data. See DOI: 10.1039/c5cy01246e

activity of the restacked nanosheet are discussed. Note that although such a structure–activity relationship has been examined in many semiconductor photocatalysts of not only metal oxides but also other types, there are very few studies that deal with the relationship found in a semiconductor photocatalyst that shows very high AQY.

2. Results and discussion

2.1. Structure of restacked $Ca_2Nb_2TaO_{10}^-$ nanosheets prepared using various agents

First, we synthesized layered $KCa_2Nb_2TaO_{10}$ crystal by the polymerized complex (PC) method according to our previous report.[5d] The details of the synthesis are described in the Experimental section. As illustrated in Scheme 1, the protonated material, $HCa_2Nb_2TaO_{10}$, was reacted with TBA^+OH^- to form a colloidal suspension containing exfoliated $Ca_2Nb_2TaO_{10}^-$ nanosheets. A transmission electron microscope (TEM) image of the exfoliated nanosheets is shown in Fig. 1, which indicates that the size of lateral dimensions of the prepared nanosheets typically ranges over several hundreds of nanometers.

The exfoliated nanosheets were then flocculated using various acids, bases, and salts. Fig. 2A shows the XRD pattern of a typical example of restacked nanosheets (here KOH-restacked material), along with data for layered $KCa_2Nb_2TaO_{10}$. The XRD pattern of the restacked sample gives very weak (00l) ($l \geq 2$) diffraction peaks, indicating that the periodic layered structure of the parent solid was lost to a large extent upon exfoliation with TBA^+OH^- and the subsequent restacking process with KOH. However, (100) and (110) diffraction peaks corresponding to in-plane diffraction are preserved in the XRD patterns. This indicates that the two-dimensional structure of perovskite sheets is preserved after the exfoliation–restacking procedure. In fact, TEM observations show that in the KOH-restacked sample, nanosheets are restacked to form aggregates while maintaining the original lateral size, as shown in Fig. 1B. It is notable that the positions of the (00l) ($l \geq 2$) diffraction peaks in the restacked nanosheets appear at lower 2θ angles than those in the corresponding layered material, suggesting more hydration of the nanosheet material.

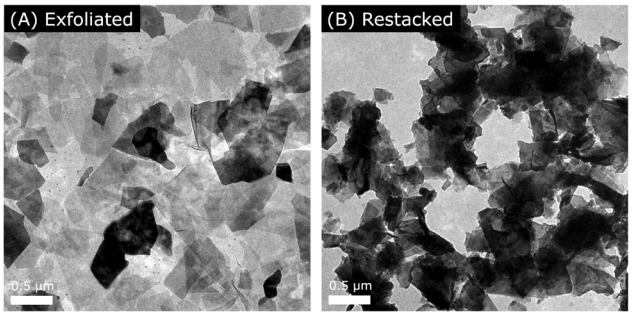

Fig. 1 TEM images of (A) TBA^+-exfoliated $Ca_2Nb_2TaO_{10}^-$ nanosheets, and (B) KOH-restacked nanosheets.

Similarly, exfoliated $Ca_2Nb_2TaO_{10}^-$ nanosheets are reassembled using ACl (A = H, Li, Na, K, Rb, Cs) as the restacking agent. As displayed in Fig. 2B, the XRD patterns of the ACl (A = H, Li, Na, K, Rb, Cs)-restacked nanosheets are similar to that of the KOH sample. However, the (00l) diffraction peaks in the NaCl sample shifted to lower 2θ angles, indicative of more hydration of the interlayer nanospace in this sample compared to others. A similar peak shift was also observed when NaOH was employed as a restacking agent (Fig. S1†). The results show that restacked nanosheets using Na^+ cations can efficiently incorporate water molecules into the interlayer gallery, even though the XRD analyses were conducted using samples after drying in an oven at 343 K overnight. This observation is consistent with the early work by Ebina *et al.*[2b] The more hydrated nature of the Na^+-restacked materials was also evidenced by thermogravimetric (TG) analysis. Fig. S2† shows TG curves for some restacked nanosheet materials, which were measured under a flow of air at 10 K min^{-1}. A mass loss observed between 300 to 473 K, which could be attributed to the volatilization of intercalated water,[14] is more pronounced in the NaCl-restacked material (weight loss: 4.2%), compared to others (2.0–2.2%).

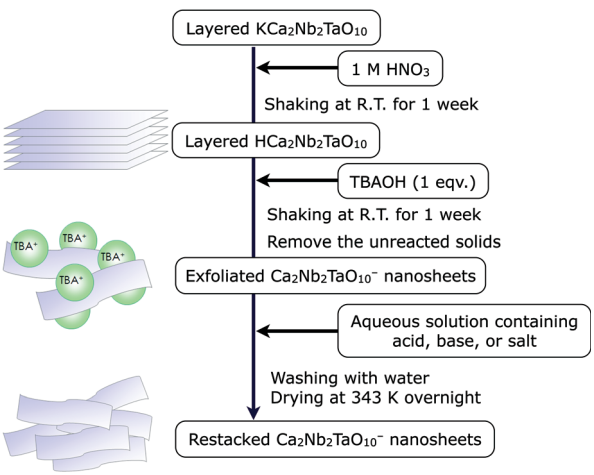

Scheme 1 Preparation of $Ca_2Nb_2TaO_{10}^-$ nanosheet aggregates using various restacking agents.

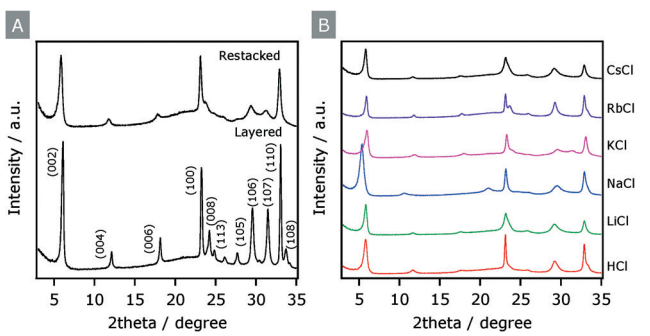

Fig. 2 XRD patterns of (A) layered $KCa_2Nb_2TaO_{10}$ and $Ca_2Nb_2TaO_{10}^-$ nanosheets restacked by KOH, and (B) $Ca_2Nb_2TaO_{10}^-$ nanosheets restacked by ACl (A = H, Li, Na, K, Rb, Cs).

As listed in Table 1, specific surface areas of restacked nanosheets were 15–30 $m^2\ g^{-1}$, much larger than that of the material before exfoliation (*ca.* 3–4 $m^2\ g^{-1}$).

To obtain more information on the local structure of restacked nanosheets accommodating different interlayer cations, Raman spectra of these samples were acquired. Fig. 3 shows Raman spectra of $Ca_2Nb_2TaO_{10}^-$ nanosheets restacked by ACl (A = H, Li, Na, K, Rb, Cs). All of the samples exhibit Raman bands at around 960–930, 775, 590, 500–450, and 320 cm^{-1}, whose assignments were made according to the previous work on the corresponding layered materials.[15] The spectral shapes of these nanosheets resemble each other, indicative of structural similarity. However, the positions of the 960–930 cm^{-1} bands, assignable to the symmetric stretching mode of the Nb–O (and/or Ta–O) terminal bond, are different. This means that the terminal bonds (most likely in the interlayer nanospace) are influenced by neighboring cations. The positions of other Raman bands, on the other hand, remained almost unchanged. Thus, while the difference in the local structure of the restacked materials was difficult to resolve by XRD, Raman spectroscopy clearly distinguished them.

We also found an exceptional case. As shown in Fig. S1,† the CsOH-restacked material showed relatively weak diffraction peak intensities compared to other AOH-restacked (A = Na, K) materials; not only diffraction peaks from (00*l*) directions but also the ones from (100) and (110), which are in-plane reflections, were relatively weak in terms of the intensity. This strongly suggests that long-range atomic ordering both in the stacking direction and in the in-plane dimension is more or less lost upon restacking with CsOH. TEM images of the CsOH restacked nanosheets are shown in Fig. S3,† which indicate that in addition to restacked sheet structures, densely aggregated larger particles having featureless morphology are present, different from the KOH-restacked one. This could explain the different features found in the XRD pattern (Fig. S1†).[16] Because CsOH is a very strong base, corrosion of the surface structure might occur on the $Ca_2Nb_2TaO_{10}^-$ nanosheets, resulting in these peculiar structural features. Thus, it was shown that restacking of $Ca_2Nb_2TaO_{10}^-$ nanosheets with different agents affects the degree of interlayer hydration and the structural form of the final material in terms of stacking order and distortion of the two-dimensional sheet.

Table 1 Specific surface areas and photocatalytic activities of $Ca_2Nb_2TaO_{10}^-$ nanosheets restacked by various agents for H_2 evolution under UV irradiation ($\lambda > 300$ nm)[a]

Entry	Restacking agent	Specific surface area/$m^2\ g^{-1}$	H_2 evolution rate[b]/μmol h^{-1}
1	HCl	29	150
2	LiCl	19	52
3	NaCl	25	58
4	KCl	25	60
5	RbCl	21	57
6	CsCl	20	53
7	NaOH	22	50
8	KOH	25	63
9	CsOH	14	38

[a] Reaction conditions: catalyst, 100 mg (0.5 wt% Pt-loaded *in situ*); 10 vol% aqueous methanol solution, 100 mL, xenon lamp (300 W); reaction vessel, Pyrex top-irradiation type. [b] Average rate in 2 h. The reproducibility was typically within 10–15%.

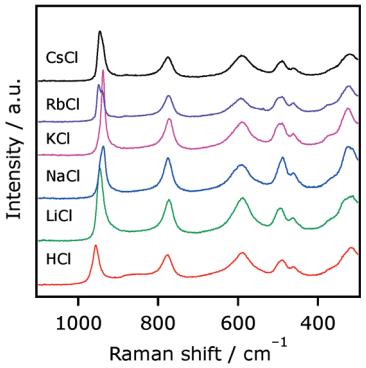

Fig. 3 Raman spectra of $Ca_2Nb_2TaO_{10}^-$ nanosheets restacked by ACl (A = H, Li, Na, K, Rb, Cs).

In contrast to XRD patterns, no significant difference could be identified in UV-visible diffuse reflectance spectra, and all of the synthesized materials exhibited a steep absorption at around 330 nm, as shown in Fig. 4. This would be reasonable because photoexcitation, from the valence band formed by oxygen 2p orbitals to the conduction band formed by the empty Nb4d and Ta5d orbitals, occurs in the two-dimensional nanosheet.

2.2. Effects of post-heating on the structure of restacked nanosheets

Post-heating of a semiconductor photocatalyst is sometimes required for modification of the photocatalyst with a cocatalyst that works as gas evolution sites, especially in an impregnation method, which requires heat treatment (typically 473–773 K) for activation of a cocatalyst.[9] However, this has rarely been investigated for nanosheet materials. Calcination of restacked nanosheets may cause a structural change due to shrinkage of the aggregated form.

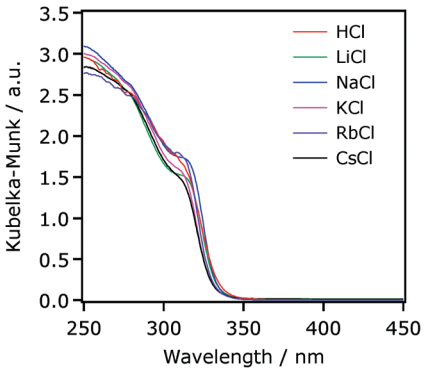

Fig. 4 Diffuse reflectance spectra of $Ca_2Nb_2TaO_{10}^-$ nanosheets restacked by ACl (A = H, Li, Na, K, Rb, Cs).

We investigated the impact of post-heating of restacked nanosheets on structural properties. To avoid topochemical dehydration,[14] here we used KOH-restacked nanosheets. With increasing temperature, the XRD peaks from (00*l*) reflections became sharper, indicating more ordering in the stacking direction (Fig. 5). In addition, the peak positions were shifted slightly to higher 2θ angles, as the temperature increased. This means that interlayer distance is reduced upon calcination, most likely due to dehydration at elevated temperatures. Interestingly, heating the KOH-restacked material at 673–873 K increased the specific surface area, as listed in Table 2. No change could be identified in the DRS (Fig. S5†). It is also noted that no significant difference was observed in the TEM image before and after post-heating (Fig. S6†).

2.3. Photocatalytic activities

Photocatalytic H_2 evolution was employed under ultraviolet (UV) light irradiation ($\lambda > 300$ nm) using the as-restacked nanosheets with the aid of a Pt cocatalyst, which was loaded by an *in situ* photodeposition method using H_2PtCl_6 as the precursor. TEM observation for Pt-photodeposited $HCa_2Nb_2TaO_{10}$ showed that Pt nanoparticles of 3–4 nm in size were deposited on the edge of the nanosheets (Fig. 6). As summarized in Table 1, the rate of H_2 evolution was dependent on the restacking agent. Restacked nanosheets prepared with ACl (A = Li, Na, K, Cs) or AOH (A = Na, K) exhibited similar activity (50–60 μmol h^{-1}). However, the rate of H_2 evolution recorded using CsOH was clearly lower than those of others (entry 9). Another exception was the HCl-restacked material, which showed the highest performance among the materials examined (entry 1). It is also noted that no correlation is observed between specific surface area and the activity of these materials. In addition, post-heating of the KOH-restacked nanosheets was found to have little impact on activity (Table 2).

2.4. Factors affecting activity

It is important to clarify factor(s) affecting the activity of a given photocatalytic material. Interlayer hydration, structural regularity (both in the stacking direction and in-plane direction), and restacking agents are possible factors that govern the H_2 evolution rate. In this work, the structural regularity both in the restacking directions (*i.e.*, *c* axis) and in the in-plane direction varied with respect to the restacking agents. In particular, using CsOH as the restacking agent resulted in lowering the structural regularity, which was evidenced by XRD and TEM analyses (Fig. S1 and S3†). As listed in Table 1, photocatalytic activity of $Ca_2Nb_2TaO_{10}^-$ sheets re-assembled by CsOH (38 ± 3 μmol h^{-1}) was slightly lower than those of others (typically 50–60 μmol h^{-1}). This result suggests that structural regularity in the stacking region and the bending of 2-D sheets both have some negative impact on activity for H_2 evolution.

It has been reported that layered metal oxide semiconductors exhibit very high photocatalytic activity for H_2 evolution under band-gap irradiation when the interlayer nanospace is hydrated and/or is available for photoredox reactions.[6a,11,12] In the present case, more hydration was observed in the NaCl- and NaOH-restacked materials compared to others (Fig. S1†). However, the activities of the two samples were much lower than that of the most active HCl-restacked material, whose interlayer nanospace is less hydrated. This clearly indicates that interlayer hydration itself is not the decisive factor for activity enhancement, and that interlayer protonation was more important than hydration. This fact in turn means that in the HCl-restacked material, reduction of protons and/or oxidation of methanol takes place more efficiently in the material

Table 2 Specific surface areas and photocatalytic activities of KOH-restacked $Ca_2Nb_2TaO_{10}^-$ nanosheets for H_2 evolution under UV irradiation ($\lambda > 300$ nm) with and without post-heating[a]

Entry	Post-heating temperature/K	Specific surface area/m^2 g^{-1}	H_2 evolution rate[b]/μmol h^{-1}
1	—	25	63
2	473	22	65
8	673	38	64
9	873	35	58

[a] Reaction conditions: catalyst, 100 mg (0.5 wt% Pt-loaded *in situ*); 10 vol% aqueous methanol solution, 100 mL, xenon lamp (300 W); reaction vessel, Pyrex top-irradiation type. [b] Average rate in 2 h.

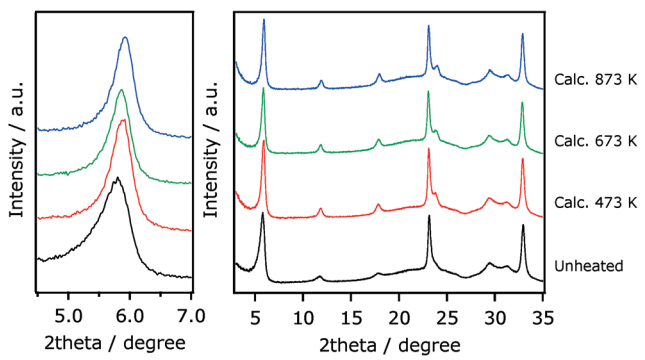

Fig. 5 XRD patterns of KOH-restacked $Ca_2Nb_2TaO_{10}^-$ nanosheets further calcined at different temperatures in air.

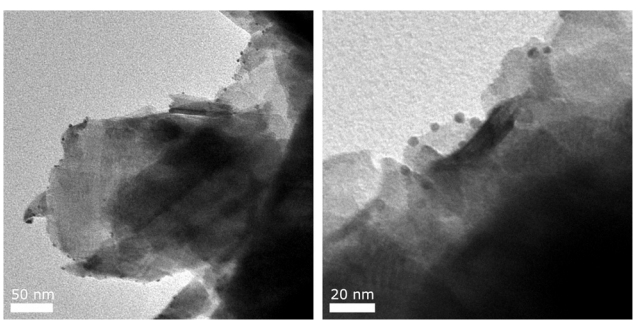

Fig. 6 TEM images of $Ca_2Nb_2TaO_{10}^-$ nanosheets restacked by HCl further photodeposited with 0.5 wt% Pt.

than in others. As shown in Fig. 6, TEM observations indicated that Pt nanoparticles, well-known catalysts for H_2 evolution, were deposited on the external surface of the restacked nanosheet, not in the interlayer nanospace, meaning that reduction of protons occurs on the external surface. It is considered that the protonated surface of the restacked nanosheet may be beneficial for proton reduction to form H_2. However, this effect may be smaller than in the interlayers; in other words, protonation may have more impact on interlayers than on the surface. Domen *et al.* have claimed that the protonated interlayer nanospace of layered $HCa_2Nb_3O_{10}$ promotes oxidation of methanol.[12] Another study reported that oxidation sites of 2-D transition metal nanosheets exist on the sheet planes, while reduction sites are located on the edge of the nanosheets,[17] consistent with the result of our TEM observation (Fig. 6). Thus, the protonation of interlayer nanospace might have a positive impact on methanol oxidation.

It was found that post-heating of KOH-restacked nanosheets in air at 873 K facilitated interlayer dehydration (Fig. 5), and increased the specific surface area (Table 2). However, the activities of the post-heated samples remained almost unchanged compared to the unheated one. This again indicates that interlayer hydration is not a decisive factor that affects photocatalytic H_2 evolution activity. Also, this result would be reasonable considering the fact that activity of the nanosheet for H_2 evolution was almost independent of the specific surface area, as can be seen in materials that were restacked using different agents.

3. Conclusions

The structure of restacked $Ca_2Nb_2TaO_{10}^-$ nanosheets was dependent on the restacking reagent employed, displaying different morphological features and different degrees of interlayer hydration. Among the materials examined, the highest activity for photocatalytic H_2 evolution from an aqueous methanol solution was obtained for the HCl material, indicating that interlayer protonation was important for enhancing activity.

4. Experimental section

4.1. Preparation of layered $KCa_2Nb_2TaO_{10}$ and subsequent proton exchange

$KCa_2Nb_2TaO_{10}$ was prepared by the polymerized complex (PC) method according to our previous report.[5d] In a typical synthesis, $NbCl_5$ (95.0%, Wako Pure Chemicals Co.) and $TaCl_5$ (90.0%, Wako Pure Chemicals Co.) powders were initially dissolved in 100 mL of methanol (99.8%, Kanto Chemicals). Next, required amounts of $CaCO_3$ (99.5%, Kanto Chemicals Co.), KCl (99.5%, Kanto Chemicals), ethylene glycol (EG; 99.5%, Kanto Chemicals), and anhydrous citric acid (CA; 98.0%, Wako Pure Chemicals) were added to the solution with stirring. The ratio of K/Ca/Nb/Ta/CA/EG was 1.1/2/2/1/30/120, where an excess of KCl (10 mol% of K) was added to the solution to compensate for volatilization of K_2O in the calcination step. The reaction mixture was heated at ~373 K on a hot plate stirrer to promote complete dissolution. The as-obtained transparent solution was heated to 400 K to promote esterification between EG and CA, yielding a glassy resin. The resin was calcined in air at 623–673 K to produce a black powder, which was then subjected to further calcination on an Al_2O_3 plate at 823 K for 4 h in air to remove the residual carbon-containing species. Finally, the resulting powder was collected and heated in air at 1373 K for 2 h in an Al_2O_3 crucible (ramp rate: 10 K min^{-1}).

Proton-exchange was carried out in aqueous nitric acid (1 M) at room temperature for 1 week. The product ($HCa_2Nb_2TaO_{10}$) was isolated by centrifugation, washing, and finally drying at 343 K in an oven overnight.

4.2. Exfoliation of layered $HCa_2Nb_2TaO_{10}$ and restacking

Exfoliation of the as-prepared proton-exchanged material was performed using aqueous tetra(*n*-butyl)ammonium hydroxide (TBA^+OH^-; Aldrich Chemical Co., 40 wt% in H_2O) at room temperature in a similar manner to that reported by Ebina *et al.*[2a] $HCa_2Nb_2TaO_{10}$ was shaken in an aqueous solution containing TBA^+OH^- for 1 week. The molar ratio of TBA^+OH^- to exchangeable cations in the layered solids was 1.0. The separation of unreacted $HCa_2Nb_2TaO_{10}$ particles was performed by spontaneous precipitation overnight and the supernatant was used as a nanosheet suspension.

To restack the colloidal $TBA^+/Ca_2Nb_2TaO_{10}^-$ nanosheets, an aqueous solution (2 M) containing a proper acid, base, or salt was added dropwise into the nanosheets suspension. The resulting precipitates were centrifuged and washed with water several times until the pH of the supernatant became neutral. After drying in an oven overnight, the sample was ground with a mortar and pestle. FT-IR analyses indicated that no residual TBA^+ species could be identified in the as-restacked materials.

4.3. Structural characterization

The prepared materials were characterized by X-ray diffraction (XRD; MiniFlex 600, Rigaku), transmission electron microscopy (TEM; H-7650, Hitachi High-Technologies), Raman spectroscopy (NRS-3100, Jasco), and UV-visible spectroscopy (V-565, Jasco). The Brunauer–Emmett–Teller (BET) surface areas of samples were also measured, using a BELSORP-mini apparatus (BEL Japan) at liquid nitrogen temperature (77 K). TG analysis was performed using a thermogravimetric analyser (TG/DTA 6200, Seiko Instruments Co.) under a flow of nitrogen (200 mL min^{-1}) at a heating rate of 10 K min^{-1}.

4.4. Photocatalytic reactions

Reactions were carried out in a Pyrex top-irradiation vessel connected to a glass closed gas circulation system, as described in the previous papers.[18] The reaction cell was immersed in a cooling water bath, which was able to maintain the temperature of the reactor at *ca.* 293 K during the

reaction. 100 mg of the restacked material was dispersed in pure water containing 10 vol% methanol (100 mL) and a proper amount of H_2PtCl_6, followed by degassing and irradiation with ultraviolet light ($\lambda > 300$ nm) from a 300 W xenon lamp (Cermax, PE300BF) with an output current of 20 A for 2 h at room temperature. Here, Pt nanoparticle cocatalysts (0.5 wt% as the metallic basis) were *in situ* loaded onto the as-prepared restacked nanosheets.[19] The evolved gases were analyzed by gas chromatography (Shimadzu, GC-8A with a TCD detector and a MS-5A column, argon carrier gas).

Acknowledgements

The authors thank Ryouhei Noma and Prof. Michikazu Hara (Tokyo Institute of Technology) for assistance in Raman measurements. This work was supported by the ENEOS Hydrogen Trust Fund, a Grant-in-Aid for Scientific Research on Innovative Areas (Project No. 25107512; AnApple), and the PRESTO/JST program "Chemical Conversion of Light Energy".

Notes and references

1 M. Osada and T. Sasaki, *Adv. Mater.*, 2012, **24**, 210–228.
2 (*a*) Y. Ebina, T. Sasaki, M. Harada and M. Watanabe, *Chem. Mater.*, 2002, **14**, 4390–4395; (*b*) Y. Ebina, N. Sakai and T. Sasaki, *J. Phys. Chem. B*, 2005, **109**, 17212–17216; (*c*) Y. Ebina, K. Akatsuka, K. Fukuda and T. Sasaki, *Chem. Mater.*, 2012, **24**, 4201–4208.
3 (*a*) S.-M. Paek, H. Jung, Y.-J. Lee, M. Park, S.-J. Hwang and J.-H. Choy, *Chem. Mater.*, 2006, **18**, 1134–1140; (*b*) T. W. Kim, S. G. Hur, S.-J. Hwang, H. Park, W. Choi and J.-H. Choy, *Adv. Funct. Mater.*, 2007, **17**, 307–314; (*c*) J. L. Gunjakar, T. W. Kim, H. N. Kim, I. Y. Kim and S.-J. Hwang, *J. Am. Chem. Soc.*, 2011, **133**, 14998–15007.
4 (*a*) O. C. Compton, E. C. Carroll, J. Y. Kim, D. S. Larsen and F. E. Osterloh, *J. Phys. Chem. C*, 2007, **111**, 14589–14592; (*b*) M. R. Allen, A. Thibert, E. M. Sabio, N. D. Browning, D. S. Larsen and F. E. Osterloh, *Chem. Mater.*, 2010, **22**, 1220–1228; (*c*) E. M. Sabio, R. L. Chamousis, N. D. Browning and F. E. Osterloh, *J. Phys. Chem. C*, 2012, **116**, 3166–3170.
5 (*a*) K. Maeda, M. Eguchi, W. J. Youngblood and T. E. Mallouk, *Chem. Mater.*, 2009, **21**, 3611–3617; (*b*) K. Maeda and T. E. Mallouk, *J. Mater. Chem.*, 2009, **19**, 4813–4818; (*c*) T. Oshima, O. Ishitani and K. Maeda, *Adv. Mater. Interfaces*, 2014, **1**, 1400131; (*d*) K. Maeda, M. Eguchi and T. Oshima, *Angew. Chem., Int. Ed.*, 2014, **53**, 13164–13168; (*e*) T. Oshima, D. Lu, O. Ishitani and K. Maeda, *Angew. Chem., Int. Ed.*, 2014, **54**, 2698–2702.
6 (*a*) H. Hata, Y. Kobayashi, V. Bojan, W. J. Youngblood and T. E. Mallouk, *Nano Lett.*, 2008, **8**, 794–799; (*b*) R. Ma, Y. Kobayashi, W. J. Youngblood and T. E. Mallouk, *J. Mater. Chem.*, 2008, **18**, 5982–5985.
7 (*a*) Y. Okamoto, S. Ida, J. Hyodo, H. Hagiwara and T. Ishihara, *J. Am. Chem. Soc.*, 2011, **133**, 18034–18037; (*b*) S. Ida, Y. Okamoto, M. Matsuka, H. Hagiwara and T. Ishihara, *J. Am. Chem. Soc.*, 2012, **134**, 15773–15782; (*c*) S. Ida, A. Takashiba, S. Koga, H. Hagiwara and T. Ishihara, *J. Am. Chem. Soc.*, 2014, **136**, 1872–1878; (*d*) S. Ida, S. Koga, T. Daio, H. Hagiwara and T. Ishihara, *Angew. Chem., Int. Ed.*, 2014, **53**, 13078–13082.
8 T. Nakato, T. Fujita and E. Mouri, *Phys. Chem. Chem. Phys.*, 2015, **17**, 5547–5550.
9 K. Maeda, *J. Photochem. Photobiol., C*, 2011, **12**, 237–268.
10 J. Zhang, Y. Chen and X. Wang, *Energy Environ. Sci.*, 2015, DOI: 10.1039/C5EE01895A, in press.
11 (*a*) A. Kudo, A. Tanaka, K. Domen, K. Maruya, K. Aika and T. Onishi, *J. Catal.*, 1988, **111**, 67–76; (*b*) A. Kudo, K. Sayama, A. Tanaka, K. Asakura, K. Domen, K. Maruya and T. Onishi, *J. Catal.*, 1989, **120**, 337–352.
12 K. Domen, J. Yoshimura, T. Sekine, A. Tanaka and T. Onishi, *Catal. Lett.*, 1990, **4**, 339–344.
13 C. Tagusagawa, A. Takagaki, S. Hayashi and K. Domen, *J. Am. Chem. Soc.*, 2008, **130**, 7230–7231.
14 M. Fang, C. H. Kim and T. E. Mallouk, *Chem. Mater.*, 1999, **11**, 1519–1525.
15 (*a*) J.-M. Jehng and I. E. Wachs, *Chem. Mater.*, 1991, **3**, 100–107; (*b*) S.-H. Byeon and H.-J. Nam, *Chem. Mater.*, 2000, **12**, 1771–1778.
16 In this case, however, no noticeable difference could be identified in the Raman spectra (Fig. S4†).
17 Y. Matsumoto, S. Ida and T. Inoue, *J. Phys. Chem. C*, 2008, **112**, 11614–11616.
18 K. Maeda, M. Higashi, D. Lu, R. Abe and K. Domen, *J. Am. Chem. Soc.*, 2010, **132**, 5858–5868.
19 B. Kraeutler and A. J. Bard, *J. Am. Chem. Soc.*, 1978, **100**, 4317–4318.